Electrochemistry

International Edition: DOI: 10.1002/anie.201602708
German Edition: DOI: 10.1002/ange.201602708

Induced Potential in Porous Carbon Films through Water Vapor Absorption

*Kang Liu[+], Peihua Yang[+], Song Li[+], Jia Li, Tianpeng Ding, Guobin Xue, Qian Chen, Guang Feng, and Jun Zhou**

Abstract: *Sustainable electrical potential of tens of millivolts can be induced by water vapor adsorption on a piece of porous carbon film that has two sides with different functional group contents. Integrated experiments, and Monte Carlo and ab initio molecular dynamics simulations reveal that the induced potential originates from the nonhomogeneous distribution of functional groups along the film, especially carboxy groups. Sufficient adsorbed water molecules in porous carbon facilitate the release of protons from the carboxy groups, resulting in a potential drop across the carbon film because of the concentration difference of the released free protons on the two sides. The potential utilization of such a phenomenon is also demonstrated by a self-powered humidity sensor.*

The intense exploration of nanotechnology has advanced traditional energy-generation technologies including photovoltaics,[1] piezoelectrics,[2] thermoelectrics,[3] and has inspired new power-generation approaches such as triboelectrics.[4] Recently, electrical potential/current generation arising from solid–liquid or solid–gas interactions has attracted increasing attention both in academia and industry. Voltage generation resulting from ionic or nonionic flows inside and outside CNTs or on graphene and liquids have previously been reported.[5–10] Several underlying mechanisms have been proposed, such as electron drag, pulsating asymmetric thermal ratchets, mutual coupling of water dipoles and free charge carriers, but an overall mechanism has not been agreed on.[5,11,12] Flows of nonpolar gases such as argon, nitrogen, and oxygen over CNTs at the speed of a few meters per second can also generate voltage and current; the underlying mechanism is assumed to be an interplay between Bernoulli's principle and the Seebeck effect.[13,14] Additionally, environmental humidity change has proved to produce transient potential in different approaches.[15–18] However, almost all the above-mentioned energy-generation strategies are attributed to liquid/gas flow or changes in environmental conditions. Herein we report that electrical potential can be induced by a natural and ubiquitous phenomenon, namely vapor adsorption, by manipulation of the proton-donating functional groups on a piece of porous carbon film (PCF). It is demonstrated that vapor adsorption in the PCF with dissimilar amounts of proton-donating groups on the two sides can directly create significant electrical potential, which can be sustained by simply keeping the PCF in a high-humidity environment.

The experimental setup for measuring the adsorption-induced potential is illustrated in Figure 1 a (Experimental details are given in the Supporting Information). To fabricate the device shown in Figure 1 b, a piece of PCF is patterned on an Al_2O_3 ceramic plate by using the blade-coating method. Scanning electron microscopy (SEM) images show that the as-fabricated PCF consists of aggregated carbon nanoparti-

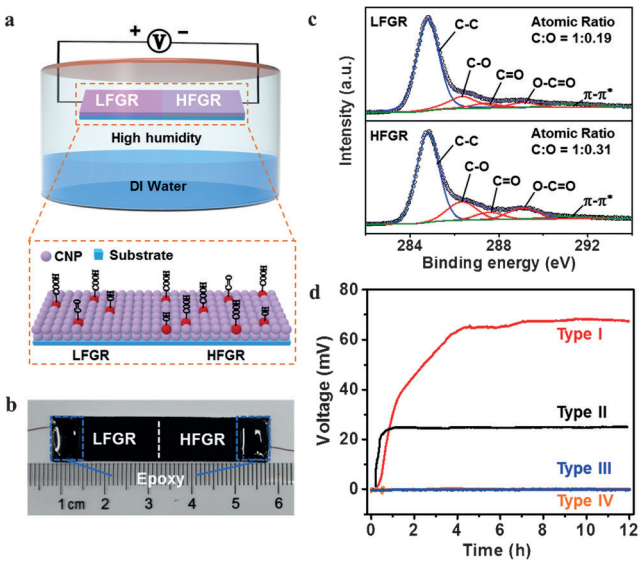

Figure 1. Porous carbon film device for harvesting adsorption-induced potential. a) Experimental setup. b) Carbon film device. HFGR denotes the region functionalized by plasma treatment, which has higher content of oxygen-containing functional groups; LFGR denotes the untreated region, which has lower content of functional groups compared to HFGR. c) XPS spectra of the plasma-functionalized (top) and pristine (bottom) PCF. The reduced C:O ratio of HFGR indicates that the proportion of oxygen-containing functional groups increases after plasma treatment. d) Open-circuit voltage generated by vapor adsorption. Device types I, II, III, and IV correspond to the PCF sample with a half region functionalized by plasma, the sample with a half region functionalized by acid, the sample with the full region functionalized by plasma, and the sample without any plasma or acid treatment, respectively.

[*] Dr. K. Liu,[+] P. Yang,[+] J. Li, T. Ding, G. Xue, Q. Chen, Prof. J. Zhou
Wuhan National Laboratory for Optoelectronics and School of Optical and Electronic Information
Huazhong University of Science and Technology
Wuhan 430074, Hubei (P.R. China)
E-mail: jun.zhou@mail.hust.edu.cn
Dr. S. Li,[+] Prof. G. Feng
State Key Laboratory of Coal Combustion, School of Energy and Power Engineering, Huazhong University of Science and Technology
Wuhan 430074, Hubei (P.R. China)
[+] These authors contributed equally to this work.

Supporting information for this article can be found under: http://dx.doi.org/10.1002/anie.201602708.

cles with diameters of tens of nanometers (Figure S1) that form a specific surface area of approximately 164 $m^2 g^{-1}$ (Figure S2). Since the PCF experiences an annealing process at 350 °C in air during the fabrication, it contains a certain amount of oxygen-containing functional groups,[19,20] as evidenced by X-ray photoelectron spectroscopy (XPS; Figure 1c). We further functionalized the PCF by simply exposing one half of the PCF to air plasma at the power of 150 W for one minute and covering the other half with polyethylene (PE) film during the process, which endows the plasma-treated region with a higher content of oxygen-containing functional groups, predominantly –COOH (Table S1), and thus increases the hydrophilicity (Figure S1). As-processed PCF hence possesses a high-functional-group region (HFGR) and a low-functional-group region (LFGR) on the two sides (i.e., two contacting halves of a PCF), while the structure and morphology of the two regions are almost the same, as demonstrated in additional Raman and Brunauer–Emmett–Teller (BET) characterization (Figures S1–3).

With the prepared PCF in hand, we fabricated a device (size = 5×1 cm^2; resistance ≈ 42.2 MΩ) as shown in Figure 1b. Two copper wires connecting the two ends of the PCF for electrical measurement were covered by epoxy resin to avoid exposure to vapor. When the device was subjected to high relative humidity (RH > 95%) by sealing it in a beaker containing water (Figure 1a), a surprisingly immediate open-circuit voltage between the two ends was detected, without any external field contribution or mechanical energy input (Figure 1d, Type I). The voltage increased gradually until reaching a maximum and then remained at a constant value of approximately 68 mV for over 6 hours at fixed RH value, which essentially differs from the electricity-generation strategy reported previously,[16,17] where the change of RH value is a prerequisite during electricity-generation process. The short-circuit current under the same condition increases to a maximum of around 3 nA and then decreases to zero within 4 hours (Figure S4). To verify this interesting observation, two different sets of experiments were carried out. In one set, the PCF with its HFGR prepared by chemical oxidation also exhibits the capability of electrical voltage generation (Figure 1d Type II, Figure S5), although the induced voltage is slightly lower than the electrical potential generated by plasma-treated samples, which is attributed to the difference in the functional-group contents of HFGRs processed by plasma treatment and chemical oxidation, respectively (Tables S1, S2). In the other set, the PCF with the whole region treated by plasma (Figure 1d, Type III) or untreated (Figure 1d, Type IV) were examined for comparison. Neither of them can induce significant electrical potential. Hence, these two sets of experiments prove that the voltage generation is related to the dissimilar functional-group contents on the two sides of the PCF.

To identify the factors that influence the induced potential, we investigated the effects of environmental humidity and device temperature. As shown in Figure 2a, the device produces a voltage of approximately 50 mV in a sealed beaker, and it decreases to zero when the beaker is unsealed and the relative humidity decreases to below 83%. Such sealing- and unsealing-induced voltage is completely reproducible (Figure 2a), thus indicating a strong correlation between the induced voltage and the relative humidity. To scrutinize the quantitative relation between the voltage and RH value, we measured the steady-state voltage of the device at different humidities. As seen in Figure 2b, the voltage remains at zero at low humidity, starts to rise at 94% RH and reaches a maximum when the humidity approaches saturation. The trend is similar to the isothermal curve of water vapor adsorption in the PCF.[21] Based on the above observations, it was necessary to investigate how the induced voltage changes when the vapor condensation occurs. We reduced the temperature of the PCF after saturated adsorption, and found that the induced voltage decreased dramatically when obvious condensation occurred (Figure S6). The explanation will be given below. The effect of temperature on the generated potential was also examined by tuning the device temperature, as shown in Figure 2c. The generated voltage was observed to vanish quickly when the temperature increased by approximately 8 °C (Figure 2c). The voltage returned to its initial value as the device temperature dropped back to room temperature. Such a voltage variation was also reproducible as the temperature changed. Meanwhile, the steady-state voltages of the device at different temperatures were measured (Figure 2d). Similar to the trend shown in Figure 2b, the voltage remained at zero in the high-temperature region and increased sharply when the temperature approached room temperature.

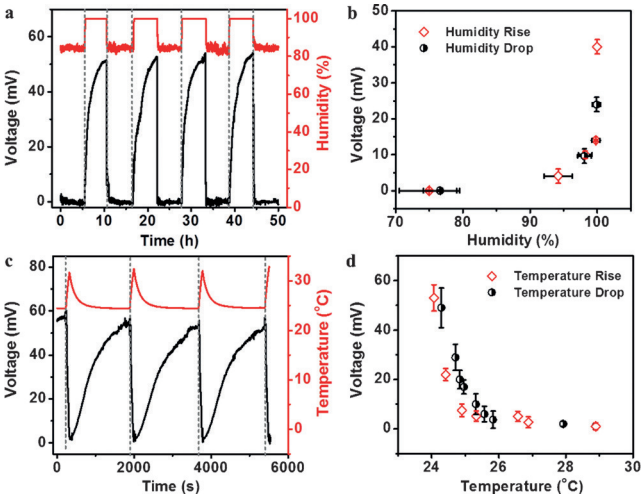

Figure 2. Condition-dependent electrical potential. a) Measured voltage of the device when the beaker was periodically sealed and unsealed. b) Steady-state potential at different humidities. c) Voltage variation when the sample was periodically heated and cooled. Temperature increase of 8 °C can theoretically result in 38% reduction in relative humidity according to the difference in saturated vapor pressures of water at 24 °C (3 kPa) and 32 °C (4.8 kPa). d) Steady-state potential at different temperatures.

These results show that the voltage generation is a spontaneous process that depends on the different sorts of functional groups on the two sides of the PCF and the high environmental humidity, which has not been clearly illustrated to date. Thus it is of great importance to understand the underlying mechanism. In our experiments, only the water

vapor and the PCF are involved, thus it is reasonable to attribute the induced voltage to the vapor adsorption, considering the consistent trends in the variation of generated voltage and adsorption capacity as a function of RH, as suggested in Figure 2b. To verify this assumption, we measured the water vapor adsorption capability of HFGR and LFGR of the PCF, as shown in Figure 3a. Since the

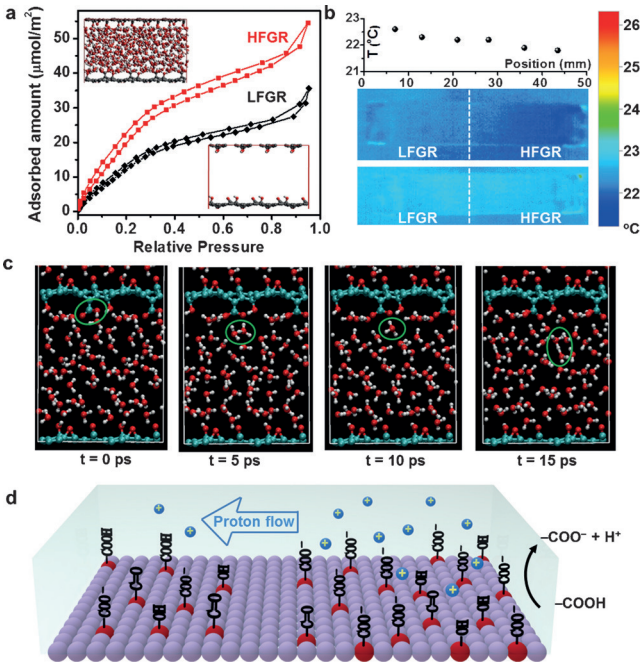

Figure 3. Origin of the adsorption-induced potential. a) Vapor adsorption isotherms recorded at 25 °C. Insets show the adsorption of a representative porous carbon model with functional-group content similar to plasma-treated (top) and pristine PCF (bottom) in experiments. b) IR images of the device at the beaker was unsealed (center) and in steady-state conditions under ambient humidity (bottom). The top graph shows the temperature distribution on the device of the center image. c) Snapshots from AIMD simulations display the process of proton release from –COOH groups of the porous carbon and proton transfer through water bridges (marked by green circles). d) Schematic of proposed mechanism for the adsorption-induced potential.

functional groups on carbon nanoparticles can promote the adsorption effectively, the HFGR thus exhibits higher water-adsorption capacity, leading to an adsorption difference along the PCF. This phenomenon was supported by grand canonical Monte Carlo (GCMC) simulation where HFGR exhibits obviously higher water-adsorption capacity than LFGR (Figure 3a inset and Figure S7–9). Figure 3b shows the infrared (IR) images of the device recorded about five seconds after unsealing the beaker, in which HFGR exhibits apparent lower temperature than LFGR after desorption, thus suggesting the stronger affinity of HFGR than LFGR for water since desorption is an endothermic process.

Even though there is a difference in quantities of adsorbed water inside porous carbons with different functional groups, it is still unclear how the observed voltage is generated by vapor adsorption. The possibility of a thermoelectric effect caused by the ununiformed temperature distribution arising from vapor adsorption is ruled out, because the measured Seebeck coefficient of the PCF is only approximately $-16\ \mu V K^{-1}$ (Figure S10), much smaller than that required for creating the electric potential observed above. Additionally, it has not been reported to date that water molecules can serve as electron donors for carbon materials;[22–24] this behavior may result in electron/hole imbalance along the PCF in our experiments. To eliminate this effect, an experiment was carried out in which the PCF was fabricated with one half hydrophilic and the other half hydrophobic. Although there is an apparent adsorption difference between the two sides, no significant electrical potential was generated (Figure S11). Furthermore, profilometer tests indicate that almost no deformation is observed when water molecules adsorb on the PCF (Figure S12), thus the possibility of potential generation induced by mechanical deformation that has been previously reported[15,18,25] is also eliminated in this work. It seems that no reported physical effects can explain the induced potential observed in our work, thus we performed ab initio molecular dynamics (AIMD) simulation using representative porous carbon models to reveal the origins of the potential. The results show that the water molecules adsorbed in porous carbon can facilitate the release of protons from –COOH groups (Figure 3c and Supplementary Movie 1). The protons can be freely transported through a bridge formed from adsorbed water molecules in porous carbon, while the $–COO^-$ group on the carbon surface remains negative. Based on the above observations, we propose the following mechanism as illustrated in Figure 3d: HFGR with more –COOH functional groups and LFGR with fewer –COOH functional groups constitute two halves of a device; more water molecules are adsorbed in HFGR, which leads to a larger amount of protons released. The imbalance of released protons in the two halves of the device results in significant difference in proton concentration, which drives proton transfer from HFGR to LFGR. After reaching a steady state, the HFGR exhibits a negative potential because of the presence of more $–COO^-$ groups on the carbon surface and reduced proton concentration, while the LFGR exhibits positive potential, as shown by our experiments in Figure 1.

According to the mechanism outlined above, the voltage is generated from two consecutive processes: proton release and proton transport. These processes are both restricted by the amount of adsorbed water molecules. AIMD modeling revealed that a small amount of water molecules could barely facilitate the proton release from the –COOH groups and form an effective water bridge for proton transport (Figure S13), which explains why the voltage is only generated at very high relative humidity. The device can also be treated as a vapor-adsorption-triggered generator that makes use of the proton concentration gradient generated by vapor adsorption. The eventual steady-state voltage is a balance of free-proton transport driven by the concentration difference and the induced electrical potential, which can be mathematically described as:[26]

$$D\,e\,\partial n/\partial x = \sigma\,\partial U/\partial x \qquad (1)$$

where D is the diffusion coefficient of protons in adsorbed water layer, e is the unit electric charge, $\partial n/\partial x$ is the concentration gradient of protons, σ is the electrical conductivity of the adsorbed water layer, and $\partial U/\partial x = \Delta U/l$ is the voltage-drop gradient along the device. According to the mechanism interpreted above and Equation (1), the generated voltage will keep constant at steady state and decrease gradually to zero when the concentration gradient disappears after desorption. Such a conclusion is supported by the results in Figure 1 d and Figure 2 a, but fundamentally different from the results reported previously where the voltage signals consist of positive and negative pulses.[16,17]

According to Equation (1), it can be concluded that the voltage is proportional to the proton concentration gradient and does not change with the device length or width, which was verified by altering the length/width of the device (Figure S14). Equation (1) also indicates that the voltage will increase when the difference in the amounts of adsorbed water and the number of protons released from the HFGR and LFGR is increased. However, when the surface water molecules are condensed, the voltage will decrease because of the dramatically reduced proton concentration and the consequent proton concentration gradient along the PCF. Hence such an adsorption-induced potential is a unique interfacial phenomenon existing in thin water layers or clusters, such as the case of adsorbed vapor in porous medium, which supports the hypothesis that water vapor condensation reduces the electrical potential (Figure S6). The "trigger" humidity, that is, the humidity under which the voltage starts to occur, is determined by the amount of adsorbed water molecules, which accounts for the proton release as well as the water bridge formation. Thus the "trigger" humidity is believed to be tunable by choosing materials with varying sensitivities to moisture. The adsorption-induced potential has also been found in other porous carbon materials including MWCNT films and acetylene carbon nanoparticle films (Figure S15), with different electrical potentials generated, thus indicating that the adsorption-induced potential is a universal phenomenon applicable for different kinds of porous carbon materials, whenever there is a functional group gradient.

A self-powered humidity sensor (Figure 4) demonstrated the potential utilization of such a phenomenon. Figure 4 a shows the schematic of such a humidity sensor, which can spontaneously output significant DC voltage when the functionalized PCF is exposed to high RH vapor. We fabricated 16 pieces of as-functionalized PCF ($2 \times 2\ cm^2$) on a piece of ceramic substrate ($10 \times 10\ cm^2$; Figure 4 b and Figure S16). Each piece of the PCF can generate voltage at high humidity, thus forming a humidity sensor array. The performance of the sensors was tested by exposing the array to air with RH > 95 %. As shown in Figure 4 c, d, an immediate potential response can be detected when wet air is present. Such a self-powered humidity sensor may be useful for mapping high-humidity areas in future industrial applications.

To conclude, we have shown that vapor adsorption on porous carbon film with different functional-group contents can induce sustainable electric potential. With the help of combined experimental studies and computational modeling, the induced potential is attributed to the free-proton transfer driven by the proton concentration difference caused by the imbalance of oxygen-containing functional groups and vapor adsorption. The unique phenomenon observed in this study may be utilized in the design of self-powered sensors, and provides new prospects for adsorption-sensitive materials.

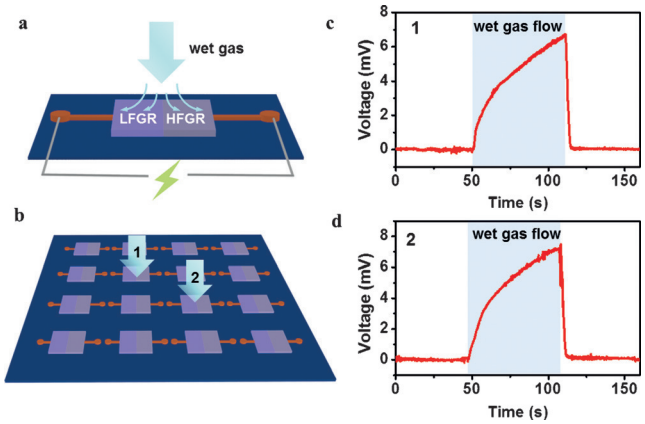

Figure 4. Application of adsorption-induced potential. a) Schematic of a humidity sensor unit. The sensor can output an obvious continuous voltage signal in the presence of very humid air. b) Illustration of an integrated self-powered humidity sensor array. c, d) Induced voltage signal when the marked locations on the sensor array are under high humidity.

Acknowledgements

This work was financially supported by the National Natural Science Foundation of China (51322210, 61434001, 51406060), the National Program for Support of Top-notch Young Professionals, the China Postdoctoral Science Foundation (2015M570639), the Fundamental Research Funds for the Central Universities (HUST: 2015MS004) and Director Fund of WNLO. We thank the facility support of the Center for Nanoscale Characterization & Devices, WNLO-HUST and the Analysis and Testing Center of Huazhong University of Science and Technology. The simulation work was carried out at National Supercomputer Center in Tianjin, and the calculations were performed on TianHe-1(A).

Keywords: adsorption · humidity · porous carbon · proton transfer

How to cite: *Angew. Chem. Int. Ed.* **2016**, *55*, 8003–8007
Angew. Chem. **2016**, *128*, 8135–8139

[1] M. Law, L. E. Greene, J. C. Johnson, R. Saykally, P. Yang, *Nat. Mater.* **2005**, *4*, 455–459.
[2] Z. L. Wang, J. Song, *Science* **2006**, *312*, 242–246.
[3] B. Poudel, Q. Hao, Y. Ma, Y. Lan, A. Minnich, B. Yu, X. Yan, D. Wang, A. Muto, D. Vashaee, *Science* **2008**, *320*, 634–638.
[4] Y. Zi, S. Niu, J. Wang, Z. Wen, W. Tang, Z. L. Wang, *Nat. Commun.* **2015**, *6*, 8376.
[5] S. Ghosh, A. Sood, N. Kumar, *Science* **2003**, *299*, 1042–1044.

[6] Z. Liu, K. Zheng, L. Hu, J. Liu, C. Qiu, H. Zhou, H. Huang, H. Yang, M. Li, C. Gu, *Adv. Mater.* **2010**, *22*, 999 – 1003.
[7] B. Persson, U. Tartaglino, E. Tosatti, H. Ueba, *Phys. Rev. B* **2004**, *69*, 235410.
[8] P. Dhiman, F. Yavari, X. Mi, H. Gullapalli, Y. Shi, P. M. Ajayan, N. Koratkar, *Nano Lett.* **2011**, *11*, 3123 – 3127.
[9] S. Ho Lee, Y. Jung, S. Kim, C.-S. Han, *Appl. Phys. Lett.* **2013**, *102*, 063116.
[10] S. Ho Lee, D. Kim, S. Kim, C.-S. Han, *Appl. Phys. Lett.* **2011**, *99*, 104103.
[11] P. Král, M. Shapiro, *Phys. Rev. Lett.* **2001**, *86*, 131.
[12] Q. Yuan, Y.-P. Zhao, *J. Am. Chem. Soc.* **2009**, *131*, 6374 – 6376.
[13] A. Sood, S. Ghosh, *Phys. Rev. Lett.* **2004**, *93*, 086601.
[14] J. Yin, J. Zhou, X. Li, Y. Chen, G. Tai, W. Guo, *Appl. Phys. Lett.* **2011**, *99*, 073103.
[15] M. Ma, L. Guo, D. G. Anderson, R. Langer, *Science* **2013**, *339*, 186 – 189.
[16] F. Zhao, H. Cheng, Z. Zhang, L. Jiang, L. Qu, *Adv. Mater.* **2015**, *27*, 4351 – 4357.
[17] F. Zhao, Y. Liang, H. Cheng, L. Jiang, L. Qu, *Energy Environ. Sci.* **2016**, *9*, 912 – 916.
[18] Q. Zhao, J. W. Dunlop, X. Qiu, F. Huang, Z. Zhang, J. Heyda, J. Dzubiella, M. Antonietti, J. Yuan, *Nat. Commun.* **2014**, *5*, 4293.
[19] S. He, P. Chen, L. Qiu, B. Wang, X. Sun, Y. Xu, H. Peng, *Angew. Chem. Int. Ed.* **2015**, *54*, 14880 – 14884; *Angew. Chem.* **2015**, *127*, 15093 – 15097.
[20] H. P. Boehm, *Carbon* **2002**, *40*, 145 – 149.
[21] T. Horikawa, T. Muguruma, D. Do, K.-I. Sotowa, J. R. Alcántara-Avila, *Carbon* **2015**, *95*, 137 – 143.
[22] R. Pati, Y. Zhang, S. K. Nayak, P. M. Ajayan, *Appl. Phys. Lett.* **2002**, *81*, 2638 – 2640.
[23] D. Tang, L. Ci, W. Zhou, S. Xie, *Carbon* **2006**, *44*, 2155 – 2159.
[24] K.-P. Yoo, L.-T. Lim, N.-K. Min, M. J. Lee, C. J. Lee, C.-W. Park, *Sens. Actuators B* **2010**, *145*, 120 – 125.
[25] P. Chen, Y. Xu, S. He, X. Sun, S. Pan, J. Deng, D. Chen, H. Peng, *Nat. Nanotechnol.* **2015**, *10*, 1077 – 1083.
[26] T. Engel, P. Reid, *Physical chemistry*, Pearson Education, San Fransisco, **2006**.

Received: March 17, 2016
Published online: May 9, 2016

